Journal of Sound and Vibration (1998) **215**(2), 331–342
Article No. sv981636

GRAVITY EFFECTS ON THE COUPLED FREQUENCIES OF A 2D FLUID–STRUCTURE PROBLEM WITH A FREE SURFACE

J.-M. Genevaux and J.-P. Brancher
Laboratoire d'Énergétique et de Mécanique Théorique et Appliquée,
2 *avenue de la forêt de Haye*, 54504 *Vandoeuvre*, *France*

and

X.-J. Chai
Wuxi Little Swan Company, 67 *Huiqian Road*, 214035 *Wuxi*, *P. R. China*

(*Received* 16 *June* 1997, *and in final form* 25 *March* 1998)

This paper discusses an experimental study of the coupled frequencies of a flexible structure partially immersed in a fluid in a finite container, in two dimensions, with non-negligible gravity effects. The results are compared with those obtained using a theoretical linear model including surface tension and meniscus length. The good agreement obtained validates this theoretical model. Curves are then presented for the coupled frequencies vs the fluid level in this container for various values of the gravity.

1. INTRODUCTION

Fluids in flexible containers behave differently from fluids in rigid ones. Space launch vehicle tanks can be considered elastic, and are partially filled with liquid. Coupled fluid–structure frequencies can therefore be crucial for the stability of this system and optimum launcher command systems must utilize a realistic model. In order to determine the effect of the major launch vehicle accelerations on the free surface, the variations of the coupled frequencies induced have to be calculated.

Rigid tanks have been investigated by Moiseev [1], Moiseev and Petrov [2], Boujot [3] and many other workers. The vibration characteristics of elastic containers are modified when they are filled with a liquid. The main difficulty in this type of problem is that neither the motion of the fluid nor the motion of the structure are known beforehand.

Fluid–structure interaction in an elastic container have been investigated extensively using various methods such as finite-element analysis, boundary-integral techniques, variational methods, and analytical methods. For an overview of numerical methods, the reader is referred to Zienkiewicz and Bettess [4], Valid and Ohayon [5], Valid *et al*. [6], Berger *et al*. [7], Morand and Ohayon [8], Boujot [3], and Schulkes [9]. For variational methods, there are Yamamoto [10] and Gupta and Hutchingson [11]. Test cases are needed to validate these numerical codes.

This paper develops such a test case for a flexible structure partially immersed in a liquid in a finite container when the effect of gravity on the free surface cannot be neglected.

The works of Caillot [12] and Veklich and Malyshev [13] neglect gravity effects on the coupled frequencies, and thus can only be used as limits of the above problem. Cylindrical

0022–460X/98/320331 + 12 $30.00/0

containers are studied in Miles [14], Bauer [15], Kana [16], Lindholm *et al*. [17], Chiba [18] and Zhou [19].

In the case of a rectangular container with elastic side walls, the variable separation method fails. Schulkes [20] gives an analytical solution for side walls considered as membranes. If the elastic side wall is treated as a beam, an analytical solution with gravity effects is proposed by Bauer *et al*. [21], but giving only the first coupled frequency. In fact, a single function is used to describe the mode shape of both the immersed part and the dry part of the beam, and this entails major discrepancies between their results and ours which are validated in section 3 of this paper.

Section 2 presents the geometrical configuration, mechanical characteristics, and the experiment performed for the test case. Section 3 summarizes the analytical solution of this problem, which was presented in detail in a preceding paper [22] for the linearized equations. Section 4 compares the analytical results of the model with experimental data, and details the procedure used to validate this approach. The coupled frequencies are then given as a function of the fluid level in the container for different values of gravity.

2. TEST CASE

The experimental geometry is presented in Figure 1. The dimensions of the rectangular container are ($L_r^* = 0{\cdot}231$ m; $L_l^* = 0{\cdot}191$ m; $L_z^* = 0{\cdot}1$ m). It is partially filled with water

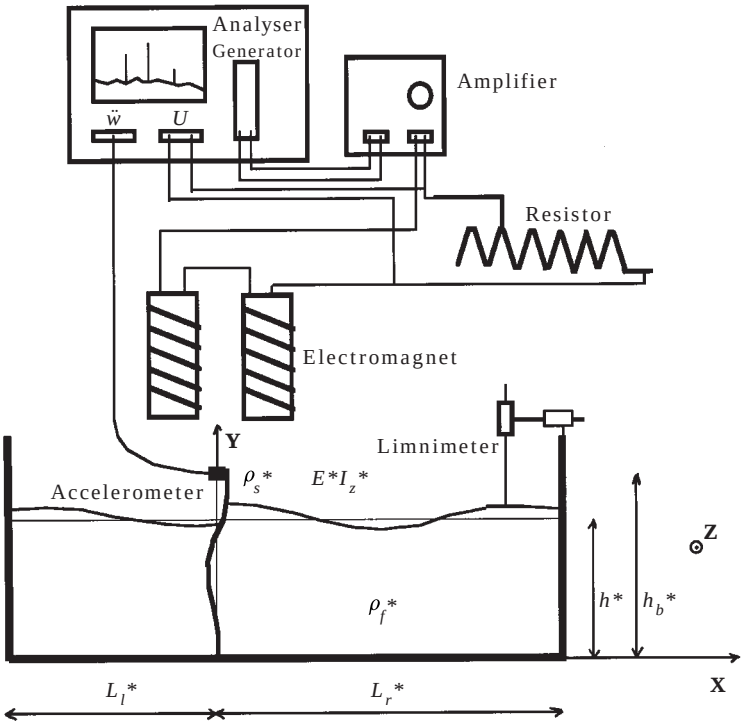

Figure 1. Cantilever beam immersed in a finite rigid container.

(h^* from 0 to 0·21 m). A cantilever plate is clamped to the bottom of the rigid container, and the top of the plate is equipped with an accelerometer and a small steel piece used to excite the system. The level of the free surface can be modified. The duraluminum plate dimensions (thickness $e^* = 0{\cdot}001$ m; length $h_b^* = 0{\cdot}311$ m; width $b^* = 0{\cdot}0995$ m) are such that its first dry bending frequency when equipped with the accelerometer, is close to the first sloshing modes of the fluid. In the **Z** direction, the gap between the plate and the container is so small that any flow between the two parts of the container can be neglected. The position of a point of the free surface is measured by limnimeter. The container wall is coated with silicone oil to limit the meniscus.

2.1. SYSTEM EXCITATION

An electromagnet placed above the structure is excited by a Bruël&Kjaër generator and amplifier. A 3·2 Ohm resistor is placed in series in the circuit. A Bruël&Kjaër analyser is used to measure the tension U between the resistor terminals. The force on the structure is proportional to the square of the electromagnet current, so that excitation frequency is twice that of the generator. The force–current ratio depends on the distance between the structure and the electromagnet, the geometric characteristics of the magnetic field, the magnetic characteristics and the size of the steel piece at the top of the plate. These parameters are kept constant throughout all the experiments. The Fourier transform of the voltage shows that the signal harmonics are negligible. The Fourier transform of U^2 is also calculated using the fundamental line of U. The amplitude of the motion $w(h_b^*, t)$; is then divided by the amplitude of $U(t)^2$. If this ratio remains constant, the linear range of the response is explored and the measure is validated. During the experiments, linear behaviour is obtained for motion amplitudes of $< \pm 3$ mm.

2.2. SYSTEM RESPONSE

The excitation is in the (**X**, **Y**) plane of Figure 1. The motion of the coupled system (fluid and structure) also occurs in this plane: so the problem can be considered as two-dimensional, and the plate can be modelled by beam equations in transverse oscillations. In the following, the "plate" will be referred to as the "beam". If the excitation induced any torsional motion in the structure or a fluid velocity field in the **Z** direction, the 2D model would not hold.

The motion of the free end of the beam is measured by an accelerometer (4370 Brüel&Kjaër) which is connected to the other channel of the analyser. The acquisition time is 64 s. The Fourier transform of the signal gives the fundamental line of the acceleration $(\partial^2 w(h_b^*, t^*))/(\partial t^{*2})$ with a precision of $\pm 0{\cdot}0156$ Hz.

The free surface is measured by a limnimeter during the accelerometer acquisition. The precision of this measurement is $\pm 0{\cdot}1$ mm.

3. MODEL

A model, similar to the one developed by Chai *et al*. [22, 23] can be developed. The fluid is non-viscous, and the amplitudes of the movement are so small that linearized solutions are possible, so potential flows are assumed to exist everywhere in the container. The motion of the structure remains perpendicular to the direction of the gravity. The potentials will be noted by ϕ_i^*. In this paper, the subscript "$\cdot r$" indicates a parameter corresponding to the right-hand side of the beam ($x^* > 0$), "$\cdot l$" for the left-hand side

($x^* < 0$). For convenience, all physical variables (denoted by superscript asterisks) are made dimensionless as follows:

$$(x, y, L_i, h_b, \eta_i, w, w_d) = \frac{(x^*, y)^*, L_i^*, h_b^*, \eta_i^*, w^*, w_d^*)}{h^*},$$

$$t = t^* \sqrt{\frac{g^*}{h^*}}, \qquad \phi(x, y, t) = \frac{\phi^*(x^*, y^*, t^*)}{h^* \sqrt{g^* h^*}}$$

in which η_i^* is the free surface elevation, w^* the transverse displacement of the beam for the immersed part, w_d^* for the dry part, t^* is the time, g^* is the gravity.

The dimensionless equations of the problem are as follows [24]:

In each fluid domain:

$$\frac{\partial_2 \phi_i}{\partial x^2} + \frac{\partial^2 \phi_i}{\partial y^2} = 0, \tag{1}$$

$$\begin{array}{ll} \text{for } i = r: & 0 \leqslant x \leqslant L_r, \qquad 0 \leqslant y \leqslant 1 \\ \text{for } i = l: & -L_l \leqslant x \leqslant 0, \qquad 0 \leqslant y \leqslant 1. \end{array}$$

On the rigid side walls of the container:

$$\frac{\partial \phi_i}{\partial x} = 0, \tag{2}$$

$$\begin{array}{ll} \text{for } i = r: & x = L_r, \qquad 0 \leqslant y \leqslant 1 \\ \text{for } i = l: & x = -L_l, \qquad 0 \leqslant y \leqslant 1. \end{array}$$

On the bottom of the container:

$$\frac{\partial \phi_i}{\partial y} = 0, \tag{3}$$

$$y = 0, \quad -L_l \leqslant x \leqslant L_r.$$

On the free-surface, the linearized boundary condition is:

$$\frac{\partial^2 \phi_i}{\partial t^2} + \frac{\partial \phi_i}{\partial y} = 0, \tag{4}$$

$$\begin{array}{ll} \text{for } i = r: & 0 \leqslant x \leqslant L_r, \qquad y = 1 \\ \text{for } i = l: & -L_l \leqslant x \leqslant 0, \qquad y = 1. \end{array}$$

On the elastic beam, the velocity compatibility condition is given by:

$$\frac{\partial \phi_i}{\partial x} = \frac{\partial w}{\partial t}, \tag{5}$$

$$x = 0, \qquad 0 \leqslant y \leqslant 1.$$

The dynamic equations differ for the wet and the dry part of the beam:

$$b_0 \frac{\partial^2 w}{\partial t^2} + \frac{\partial^4 w}{\partial y^4} = G_0 \left(\frac{\partial \phi_r}{\partial t} - \frac{\partial \phi_l}{\partial t} \right), \qquad x = 0, \qquad 0 < y < 1. \tag{6}$$

The right-hand side term of this equation represents the load applied by the liquid.

$$b_0 \frac{\partial^2 w_d}{\partial t^2} + \frac{\partial^4 w_d}{\partial y^4} = 0, \qquad x = 0, \qquad 1 < y < h_b \tag{7}$$

where $b_0 = h^{*3}\rho_s^* g^*(E^*I^*)^{-1}$; $G_0 = h^{*4}\rho_f^* g^*(E^*I^*)^{-1}$ are two dimensionless parameters that correspond to the characteristics of the beam and the liquid respectively. ρ_s^* is the linear mass density of the beam, ρ_f^* the mass density of the liquid per unit area, E^*I^* the flexure stiffness of the beam.

The boundary conditions for the beam give relations between w_d and w, as functions of the mass m^* and the rotational inertia J^* around the **Z** axis of the accelerometer and the small steel piece [25].

$$\left.\begin{aligned}
& w = 0, \qquad \frac{\partial w}{\partial y} = 0, && y = 0 \\
& \frac{\partial^2 w}{\partial y^2} = \frac{\partial^2 w_d}{\partial y^2}, \qquad \frac{\partial^3 w}{\partial y^3} = \frac{\partial^3 w_d}{\partial y^3}, && y = 1 \\
& w_d = w, \qquad \frac{\partial w_d}{\partial y} = \frac{\partial w}{\partial y}, && y = 1 \\
& \frac{\partial^2 w_d}{\partial y^2} + J\frac{\partial^3 w_d}{\partial t^2 \partial y} = 0, \qquad \frac{\partial^3 w_d}{\partial y^3} - m\frac{\partial^2 w_d}{\partial t^2} = 0, && y = h_b
\end{aligned}\right\}. \tag{8}$$

Two dimensionless parameters appear in the boundary condition equations at the extremity of the beam $m = (G_0 m^*)/(\rho_f^* h^{*2})$; $J = (G_0 J^*)/(\rho_f^* h^{*4})$.

The method for solving this set of equations was given by Chai [24]. The form of the solution is briefly as follows:

For the potentials,

$$\phi_i(x, y) = \left(\beta \frac{\cos[q(x-1)]}{\sin(q)} \cosh(qy) + \sum_{n=0}^{\infty} \alpha_n \frac{\cosh[p_n(x-1)]}{\sinh(p_n)} \cos(p_n y)\right)\omega \sin \omega t. \tag{9}$$

For the free surfaces,

$$\eta_i(x, y) = \left(\beta q \frac{\cos[q(x-1)]}{\sin(q)} \sinh(q) - \sum_{n=0}^{\infty} \alpha_n p_n \frac{\cosh[p_n(x-1)]}{\sinh(p_n)} \sin(p_n)\right)(-\cos \omega t). \tag{10}$$

For the immersed part of the beam,

$$w = \left(\sum_{j=1}^{4} Z_j H_j(y, \omega)\right)(-\cos \omega t). \tag{11}$$

For the dry part of the beam,

$$w_d = (Z_5 \cos By + Z_6 \sin By + Z_7 \cosh By + Z_8 \sinh By)(-\cos \omega t). \tag{12}$$

The function $H_j(y, \omega)$ is given in the appendix of [2]. The parameters q and p_n are given by the following relations in which the surface tension σ^* is taken into account.

$$\omega^2 = -p_n \tan p_n(1 + p_n^2\sigma) \tag{13}$$

$$\omega^2 = q \tanh q(1 + q^2\sigma) \tag{14}$$

with,

$$\sigma = \frac{\sigma^*}{\rho_f^* h^{*2} g^*}\,. \tag{15}$$

The real quantities q, p_n, α and β, as well as the functions $H_j(y, \omega)$, depend on the angular frequency ω. For a given ω, the set of equations (8) gives the values of the Z_j (j ranging from 1 to 8). The determinant of the corresponding matrix must be zero to avoid the solution $Z_j = 0$ for any j. This relation gives the coupled angular frequencies of the model ω_{cm}. Before observing the behaviour of the model, its parameters must be defined.

The dimensionless parameters reflect the effect of the different characteristics of the system. $\sigma =$ quantifies the ratio between the surface tension phenomena and the gravity effects [equation (15)]; $b_0 =$ characterizes the ratio between the beam inertia and stiffness, using the dry frequencies of the structure [equation (7)]; $G_0 =$ characterizes the level of the fluid–structure interaction [equation (6)]; m and $J =$ quantify the effect of the accelerometer inertia on the dry frequencies [equation (8)]; $L_i =$ quantifies the ratio between the length of each container and the water depth for the side i of the beam; $h_b =$ quantifies the ratio between the length of the beam and the water depth.

4. RESULTS

The model parameters are determined and then the frequency predictions are compared to experimental data, for two water levels, to validate the model. The behaviour of the coupled frequencies with the water level is then presented.

4.1. COMPARISON OF THEORY WITH EXPERIMENT

The validity of the model is demonstrated by the following procedure. The characteristics of the dry structure model are first determined, and then the effective length of the free surfaces. Then the model parameters are completely defined and the response of the fluid–structure model are compared to experimental results for several frequencies and several water depths.

The first dry frequency of the equipped beam was measured and found to be $f_{s1} = 4{\cdot}0626 \pm 0{\cdot}0156$ Hz. This frequency depends on the characteristics of the beam and on its boundary conditions. The flexure stiffness E^*I^* of the beam was calculated to achieve this first frequency. The mass of the accelerometer and the steel piece is $m^* = 0{\cdot}05896 \pm 0{\cdot}00005$ kg. The inertia was calculated using the dimensions of the pieces, $J^* = 3{\cdot}21 \times 10^{-6} \pm 0{\cdot}03 \times 10^{-6}\,\mathrm{kg\,m^4}$. I^*, which is given by $(b^*e^{*3})/12$. The derived Young's modulus used to find f_{s1} is $E^* = 0{\cdot}6243 \times 10^{11} \pm 0{\cdot}0048 \times 10^{11}$ Pa. This value is realistic for duraluminium.

When the first two coupled frequencies for a given water level h_1^* were measured, $L_r = L_r^*/h^*$ was chosen to be close to 1 in order to get a strong coupling between the fluid and the structure. For the experiment, $h_1^* = 0{\cdot}182$ m. The first two coupled frequencies were measured to be $f_{c1}^* = 1{\cdot}8128 \pm 0{\cdot}0156$ Hz; $f_{c2}^* = 2{\cdot}0312 \pm 0{\cdot}0156$ Hz. For f_{c1}^*, the motion of the free surface η_r^* is greater than η_l^*: the mode shape for f_{c1}^* mainly concerns

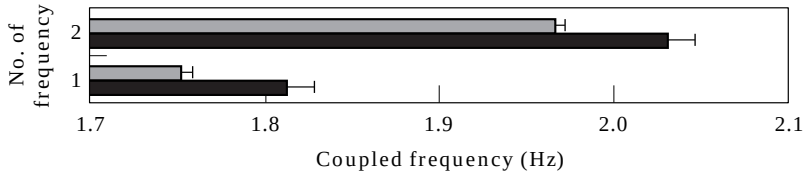

Figure 2. Comparison between coupled frequencies for the experiment (f_c) and the model (f_{cm}) without consideration of meniscus effects, for a fluid height of 0·182 m. The mean value corresponds to the bar. The accuracy of the measure or the model is also indicated. The tip indicates maximum value.

the right-hand side of the beam. For f^*_{c2}, the mode shape mainly concerns the left-hand side of the beam.

The characteristics of the fluid and of the free surface are $\rho_f^* = (1000 * 0{\cdot}1)$ kg m^{-2} and $\sigma^* = (0{\cdot}072 * 0{\cdot}1)$ N is the surface tension in the model. The factor 0·1 corresponds to the width of the container. If the real lengths of the container are used ($L_r^* = 0{\cdot}231$ m and $L_l^* = 0{\cdot}1913$ m), the calculated coupled frequencies are $f^*_{cm1} = 1{\cdot}7528 \pm 0{\cdot}0058$ Hz and $f^*_{cm2} = 1{\cdot}9668 \pm 0{\cdot}0058$ Hz. The accuracies on f^*_{cm1} and f^*_{cm2} are obtained using all the accuracies of the model parameters. The first two coupled frequencies (f^*_{cm}) calculated do not coincide with the experimental results (Figure 2). The effective length of each free surface must be shorter. The size of the meniscus at all structure free–surface interfaces seems to be of the order of 5×10^{-3} m. The strong curvature of the free surface increases its stiffness locally. The effective length of each free surface can be calculated to match the two first coupled frequencies according to their accuracy. The results are $L_r^* = 0{\cdot}2164 \pm 0{\cdot}0039$ m and $L_l^* = 0{\cdot}1799 \pm 0{\cdot}0027$ m. A meniscus influence of 0·0063 m can be considered for all the contact lines. This value reduces the experiment-model gap (Figure 3). This meniscus effect is consistent with its size.

In order to validate these effective lengths, the first twelve coupled frequencies were measured. The Bode diagram of $w(h_b)$ is presented in Figure 4. The maximum responses indicate the coupled frequencies. The calculated coupled frequencies f_{cm} are compared to the experimental ones f_c using the mean value of the effective length ($L_r^* = 0{\cdot}2184$ m and $L_l^* = 0{\cdot}1787$ m) (Figure 4). These show very good agreement except for the 4th coupled frequency. For this frequency, the discrepancy between the model and the experiment is 0·0092 Hz. This disagreement is very small compared with the frequency value. The 12th predicted frequency was not found, experimentally. But the Bode diagram (Figure 4) shows a maximum about 4·85 Hz larger than the others, so that the two maximums cannot be distinguished experimentally.

The Bode diagram for a fluid height of $h_2^* = 0{\cdot}0986$ m is plotted in Figure 5 along with the predicted coupled frequencies, f_{cm}, and the experimental frequencies f_c. The first seven frequencies are predicted well by the model. The 8th frequency of the model cannot be

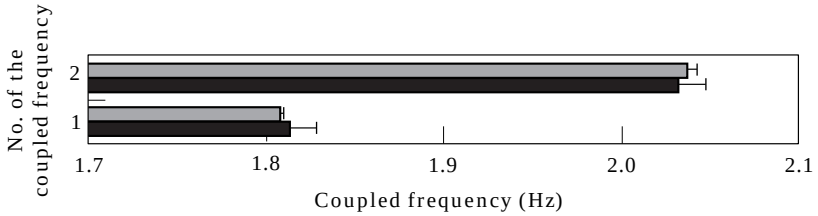

Figure 3. Comparison between coupled frequencies for the experiment (f_c) and model (f_{cm}) considering the meniscus effects of 0·0063 m, for a fluid height of 0·182 m. The accuracies of the measure and the model are also indicated.

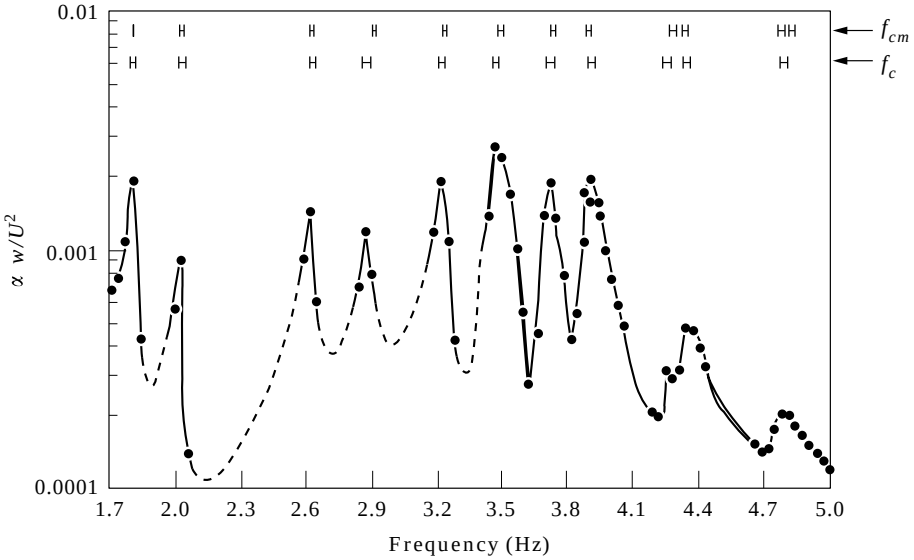

Figure 4. Experimental Bode diagram for a fluid height of $h_1^* = 0{\cdot}182$ m. The vertical axis is proportional to the ratio of the displacement of the top of the structure $w(h_b)$ to the square of the excitation tension U. f_{cm} = predicted frequencies, f_c = measured frequencies. Length of bar indicates accuracy.

detected in the Bode diagram. This experimental frequency may be masked by the major increase in the frequency response. The 9th and the 10th numerical frequencies are closer to one another than the experimental ones. These correspond to the highest frequency response. The interactions between these two close modes are not predicted by the model. The 11th and the 12th frequencies are the sloshing frequencies of the fluid in the container. The corresponding motion of the structure is smaller than the free-surface motion, so it

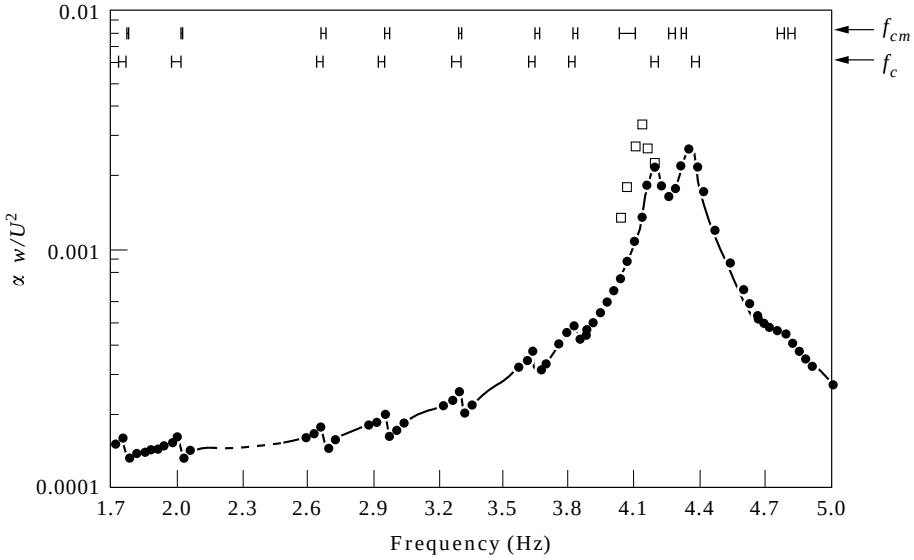

Figure 5. Experimental Bode diagram for a fluid height of $h_2^* = 0{\cdot}0986$ m. The vertical axis as in Figure 4. f_{cm}, f_c as for Figure 4 as in the meaning of the bars. ●, Small amplitude oscillation; □ large amplitude ($w > 0{\cdot}005$ m) oscillation.

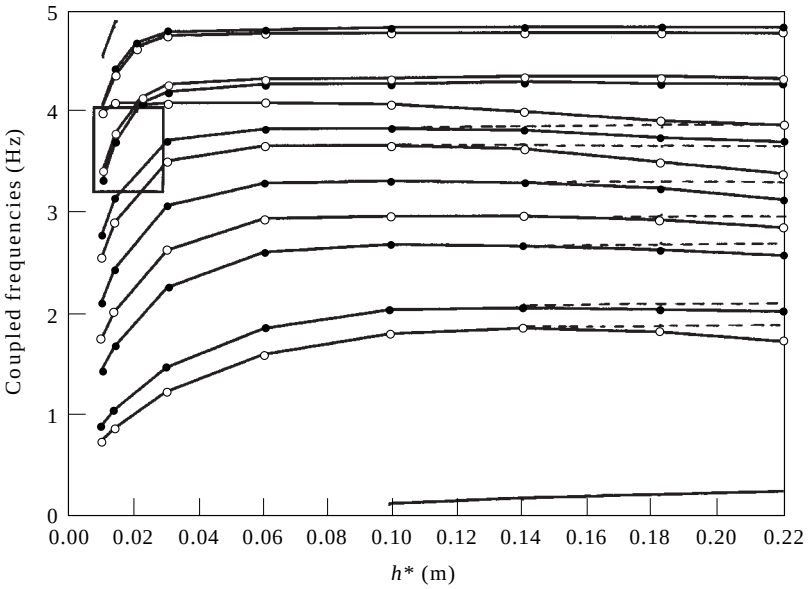

Figure 6. Variation of the coupled frequencies of the model (f_{cm}) with the height of the liquid. The sloshing frequencies in rigid containers of the same size are also plotted (dashed lines: ● (solid circle), right side f_{slr}, ○ (open circle) left side f_{sll}).

appears on the Bode diagram only as a small increase in the displacement at the extremity of the beam. If the amplitude of the excitation is increased, nonlinear effects modify the frequency response as shown on Figure 5. A nonlinear model would be useful.

4.2. VARIATION OF COUPLED FREQUENCIES WITH FLUID HEIGHT

The model can now be considered to be validated. Figure 6 gives, the variation of the coupled frequencies with the fluid height. The sloshing frequencies in containers of the same dimensions are also plotted: $f_{sll\,(left)}$, $f_{slr\,(right)}$. Figure 7 shows the coupled frequencies

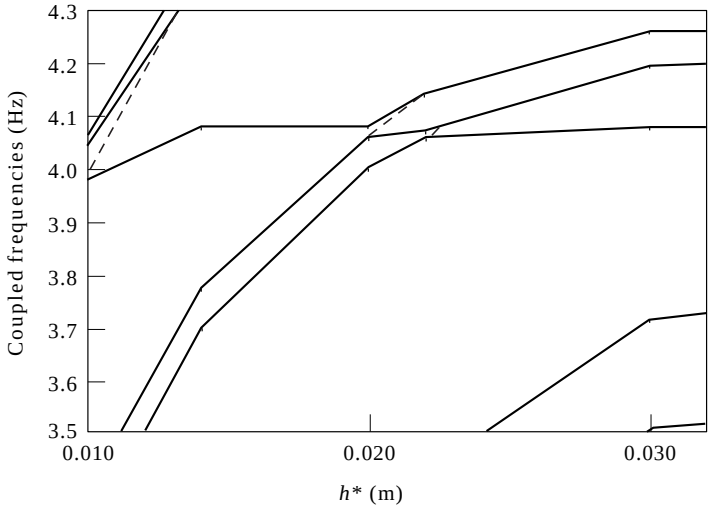

Figure 7. Variation of the coupled frequencies of the model (f_{cm}) with the height of the liquid for low water levels. The sloshing frequencies in rigid containers of the same size are also plotted (dashed lines).

for low water levels ($h^* < 0{\cdot}1$ m in the configuration). These consist of the sloshing frequencies and a frequency near the first dry frequency of the beam. Closer analysis shows that this frequency does not cut the others as the water level increases. Near 4 Hz, the coupled frequency leaves the proximity of $f_{sl\,i}$, and jumps to the proximity of $f_{sl\,i-1}$.

For higher water levels, two cases can be pointed out. Those frequencies that are greater than the first dry frequency (4 Hz), are more or less equal to the sloshing frequencies. The lower frequencies decrease as the water level rise and leave their corresponding sloshing frequencies. For a given water level, these decreases are not proportional to the distance to the dry frequency. For $h^* = 0{\cdot}182$ m, for example, the distance between f_{cm1} and f_{slr1} is greater than the distance between f_{cm2} and f_{sll1}. The ratio of the beam motion amplitude to that of the free surface increases with the distance of f_{cm} from f_{sll} and f_{slr}.

4.3. VARIATION OF COUPLED FREQUENCIES WITH GRAVITY

The dimensional time t^* is related the dimensionless time t, by

$$t^* = t\sqrt{\frac{h^*}{g^*}}, \tag{16}$$

so the coupled frequencies ω^* are related to the dimensionless frequencies ω by

$$\omega^* = \omega\sqrt{\frac{g^*}{h^*}}. \tag{17}$$

The dimensionless system is solved. If the value of g^* is changed, the only dimensionless equations that are changed are (13) and (14). The parameter σ depends on g^* [see equation (15)]. Two cases must be studied.

(1) If the surface tension is negligible compared to the gravity effects, the second terms $p_n^2\sigma$ and $q^2\sigma$ are smaller than 1 ($p_n^2\sigma \ll 1$; $q^2\sigma \ll 1$). The dimensionless frequencies are then

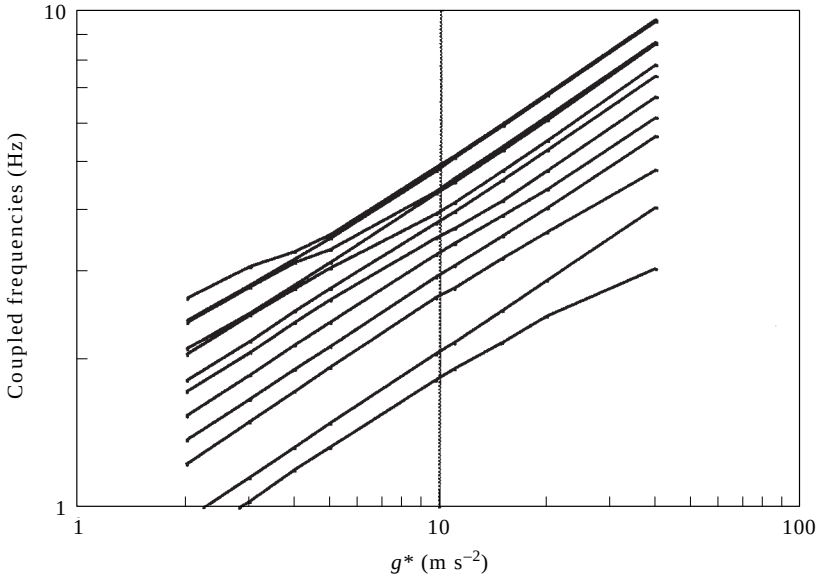

Figure 8. Variation of the coupled frequencies with g^* for a water level of 0·182 m.

independent of g^*, and the dimensional frequencies can be deduced by the above equation (17).

(2) If the surface tension is not negligible compared to the gravity effects, the dimensionless coupled frequencies are modified slightly and the dimensional frequencies are then deduced.

For a given system in a launcher whose acceleration varies for example, from g^* to 10 g^* and then returns to 0·1 g^*, each ω_{ci} remains more or less constant (as it depends on σ^*), and the corresponding dimensional frequencies vary approximately from ω_{ci}^* to $\sqrt{10}$ ω_{ci}^* and back to $\sqrt{0{\cdot}1}\ \omega_{ci}^*$. It quickly appears that the entire frequency domain will be swept by several coupled frequencies of the system with the variation of g^*. This is illustrated in Figure 8. For a water level of 0·182 m, the 11 first coupled frequencies are roughly proportional to $\sqrt{g^*}$.

5. CONCLUSION

A two-dimensional test case is presented for fluid–structure interaction where gravity effects cannot be neglected. The analytical solution of the problem is outlined, and the results are compared with experimental data. The need to take into account the surface tension of the free surface and a meniscus length of 6 mm at each solid-fluid-air line is pointed out. The analytical model is validated. The behaviour of the coupled frequencies with changes in container liquid level is then calculated. Far from the first dry frequency of the structure, the effect of the coupling is not negligible.

This problem could be used in the future as a test case for numerical codes. The nonlinear solution of this problem and the experimental measurements are presently being studied.

ACKNOWLEDGMENTS

Our thanks go to J.P. Boutrou and D. Lallement, who constructed the experimental container, and to E. Saatdjian for his help in writing this article.

REFERENCES

1. N. N. Moiseev 1964 *Advances in Applied Mechanics* **8**, 233–288. Introduction to the theory of oscillations of liquid-containing bodies.
2. N. N. Moiseev and A. A. Petrov 1966 *Advances in Applied Mechanics* **9**, 91–153. The calculation of free oscillations of a liquid in a motionless container.
3. J. Boujot 1972 *Journal de Mécanique* **11**, 649–671. Sur l'analyse des caractéristiques des vibrations d'un liquide contenu dans un réservoir.
4. O. C. Zienkiewicz and P. Bettess 1978 *International Journal for Numerical Methods in Engineering* **13**, 1–16. Fluid–structure dynamic interaction and wave forces, an introduction to numerical treatment.
5. R. Valid and R. Ohayon 1974 *La Recherche Aérospatiale* **5**, 319–325. Influence du ballottement dans les réservoirs des bouts d'ailes sur les modes propres de vibration d'un avion.
6. R. Valid, R. Ohayon and H. Berger 1974 *La Recherche Aérospatiale* **6**, 367–379. Le calcul des réservoirs élastiques partiellement remplis de liquides pour la prévision des effets POGO.
7. H. Berger, J. Boujot and R. Ohayon 1975 *Journal of Mathematical Analysis and Application* **51**, 272–298. On the spectral problem in vibration mechanics: computation of elastic tanks.
8. H. Morand and R. Ohayon 1979 *International Journal for Numerical Methods in Engineering* **14**, 741–755. Substructure variational analysis of the vibration of the coupled fluid-structure systems, finite element results.
9. R. M. S. M. Schulkes 1992 *Journal of Computational Physics* **100**, 270–283. Interaction of an elastic solid with a viscous fluid: eigenmode analysis.

10. Y. Yamamoto 1981 *International Journal in Engineering Science* **19**, 1757–1762. A variational principle of solid water interaction system.
11. R. K. Gupta and G. L. Hutchingson 1988 *Journal of Sound and Vibration* **122**, 491–506. Free vibration analysis of liquid storage tanks.
12. G. Caillot 1983 *Thèse de l'université scientifique et médicale et l'institut national polytechnique de Grenoble*. Contribution à la recherche de méthodes analytiques pour l'étude de l'influence du confinement sur la vibration des structure en présence de milieu fluide.
13. N. A. Veklich and B. M. Malyshev 1990 *Mechanics of Solids* **25**, 164–172. Vibration of an elastic plate in a rectangular volume of fluid.
14. J. W. Miles 1958 *Journal of Applied Mechanics* **25**, 277–283. On the sloshing of a liquid in a flexible tank.
15. H. F. Bauer 1963 *AIAA Journal* **1**, 2601–2606. Liquid sloshing in a cylindrical quarter tank.
16. D. D. Kana 1966 chapter 9 of *The Dynamic Behaviour of Liquid in Moving Containers*, H. N. Abramson, ed., NASA-SP-106. Interaction between liquid propellants and the elastic structure.
17. U. S. Lindholm, W. H. Chu, D. D. Kana and H. N. Abramson 1972 *AIAA Journal* **1**, 2092–2099. Bending vibrations of a circular cylindrical shell with an internal liquid with a free surface.
18. M. Chiba 1993 *Journal of Fluids and Structures* **7**, 57–73. Non-linear hydroelastic vibration of a cylindrical tank with an elastic bottom, containing liquid; Part II: linear axisymmetric vibration analysis.
19. D. Zhou 1994 *Applied Mathematics and Mechanics* **15**, 831–839. Free bending vibration of annular cylindrical tank partially filled with liquid in the consideration of surface waves.
20. R. M. S. M. Schulkes 1990 *Journal of Engineering Mathematics* **24**, 237–259. Fluid oscillations in an open flexible container.
21. H. F. Bauer, T. M. Hsu and J. T. S. Wang 1968 *ASME Journal Basic Engineering* **90**, 373–377. Interaction of a sloshing liquid with elastic containers.
22. X. Chai, J. M. Genevaux and J. P. Brancher 1996 *European Journal of Mechanics B/Fluid* **15**, 865–883. Fluid–solid interaction in a rectangular container.
23. X. Chai, J. M. Genevaux and J. P. Brancher 1995 *Proceedings of the* 12*ième Congrès Français de Mécanique*, Strasbourg septembre 1995, **4**, 77–80. Analyse d'interaction fluide–structure en milieu borné avec surface libre.
24. X. Chai 1996 *Thèse de l'INPL*, *Nancy*, 31 Octobre 96. Influence de la gravité sur les interactions fluide-structure pour un fluide dans un domaine borné à surface libre.
25. R. W. Clough and J. Penzien 1975 *Dynamics of Structures*, New York: McGraw–Hill.